Velocity and temperature measurements in a turbulent water-filled Taylor–Couette–Poiseuille system

Adrien Aubert, Sébastien Poncet, Patrice Le Gal, Stéphane Viazzo, Michael Le Bars

Velocity and temperature measurements in a turbulent water-filled Taylor–Couette–Poiseuille system

A. Aubert [a, b], S. Poncet [a, c, *], P. Le Gal [b, 1], S. Viazzo [a, 2], M. Le Bars [b, 3]

[a]Aix-Marseille Université CNRS, Ecole Centrale Marseille, Laboratoire M2P2, UMR 7340 Technopôle Château-Gombert, 38 rue F. Joliot-Curie, Marseille, France
[b]Aix-Marseille Université CNRS, Ecole Centrale Marseille, I.R.P.H.E., UMR 7342 Technopôle Château-Gombert, 49 rue F. Joliot-Curie, Marseille, France
[c]Université de Sherbrooke, Département de génie mécanique, 2500 boulevard de l'Université, Sherbrooke, Québec, Canada

Motivated by the difficulties encountered by engineers to cool down the rotating shafts of industrial machines, the present work investigates the heat and mass transfers in the rotor-stator gap of a Taylor–Couette system with an axial water flow characterized by an aspect ratio $\Gamma = 50$ and a radius ratio $\eta = 8/9$. Extensive velocity and temperature measurements have been performed on an experimental set-up for a wide range of the flow parameters: the axial Reynolds number *Re* and the Taylor number *Ta* reach the values 1.12×10^4 and 7.9×10^7 respectively. In particular, coherent structures close to the rotating wall were measured by Stereo Particle Image Velocimetry. A correlation for the Nusselt number *Nu* on the rotating wall is finally provided against the axial Reynolds, Taylor and Prandtl numbers. *Nu* is proportional to the Taylor number to the power ~0.13 close to the exponent 1/7 highlighted by an analytical model. This small exponent traduces the control of heat transfers by the rotating viscous layer and thus may explain the difficulty met by engineers to develop strategies for the effective cooling of such rotating apparatus.

1. Introduction

The present investigation concerns the heat transfer process in turbulent Taylor–Couette–Poiseuille flows. The fluid is confined between two differentially heated coaxial cylinders, with an inner rotating cylinder and an outer stationary one. An axial throughflow is supplied within the cavity. It gives rise to the competition between the rotational flow inducing radial centrifugal effects and the axially driven flow. These composite flows have many applications in process engineering (dynamic membrane filtration, rheology, UV disinfection, pasteurization) and in turbomachinery industry for bearings, asynchronous motor with axial ventilation, rotating heat exchangers and the drilling of oil wells among other things. A better knowledge of the convective heat transfer in the annular gap is generally required to optimize the performances of these rotating machineries. Often the radial gap between the cylinders is quite weak (of the order of 1 mm) and the rotation rate of the inner cylinder can reach more than 2×10^5 rpm. The difficulty to perform accurate measurements in such narrow clearances and especially in the very thin boundary layers along the cylinders has slowed down the development of specific numerical models. It explains why relatively few works have been dedicated to the study of both the hydrodynamics and the heat transfer process in such complex flows and the needs for numerical and experimental data.

The effect of an axial throughflow on a Taylor–Couette flow has been considered experimentally by Kaye and Elgar [1] in the isothermal case. Their results showed in particular the existence of four main flow regimes: laminar or turbulent, with or without Taylor vortices. These four regimes depend on the axial Reynolds number $Re_Q = \overline{V_z} D_h/\nu$ (based on the incoming fluid axial velocity $\overline{V_z}$, the hydraulic diameter $D_h = 2\Delta R = 2(b-a)$ and ν the fluid kinematic viscosity, a and b being the radii of the inner and outer cylinders respectively) and on the Taylor number $Ta = \Omega^2 a(\Delta R)^3/\nu^2$ (Ω the rotation rate of the inner cylinder). Later, Becker and Kaye [2] studied the heat transfer in the gap between a heated inner rotating

* Corresponding author. Université de Sherbrooke, Département de génie mécanique, 2500 boulevard de l'Université, Sherbrooke, Québec J1K 2R1, Canada. Tel.: +1 819 821 8000 62150.

E-mail addresses: AAubert@irphe.univ-mrs.fr (A. Aubert), Sebastien.Poncet@USherbrooke.ca (S. Poncet), legal@irphe.univ-mrs.fr (P. Le Gal), stephane.viazzo@univ-amu.fr (S. Viazzo), lebars@irphe.univ-mrs.fr (M. Le Bars).

[1] Tel.: +33 (4) 13 55 20 79.
[2] Tel.: +33 (4) 91 11 85 50.
[3] Tel.: +33 (4) 13 55 20 73.

Nomenclature

a,b	the radii of the inner and outer cylinders respectively (m)
A, B	coefficients
D_h	$=2(b-a)$, the hydraulic diameter (m)
h	length of the cylinders (m)
N	$=\Omega a/\overline{V_z}$, swirl parameter
Nu	Nusselt number (−)
Pr	$=\nu/\kappa$, Prandtl number (−)
Q	volume flow rate (m^3/s)
r,θ,z	cylindrical coordinates (m)
Re_{eff}	$=V_{eff}D_h/\nu$, effective Reynolds number (−)
Re_Q	$=\overline{V_z}D_h/\nu$, axial Reynolds number (−)
R_{ij}	Reynolds stress tensor with $i,j=(r,\theta,z)$ (m^2/s^2)
T	temperature (K)
Ta	$=\Omega^2 a(\Delta R)^3/\nu^2$, Taylor number (−)
V_{eff}	$=(\overline{V_z}^2+\alpha(\Omega a)^2)^{1/2}$, effective velocity (m/s)
v'_r, v'_θ, v'_z	fluctuating radial, tangential and axial velocity components (m/s)
V_r,V_θ,V_z	temporal mean radial, tangential and axial velocity components (m/s)
$\overline{V_z}$	spatially averaged axial velocity imposed at the inlet (m/s)
α, β, γ	coefficients
δ	boundary layer thickness (m)
ΔR	$=b-a$, radial gap (m)
η	$=a/b$, radius ratio of the cavity (−)
Γ	$=h/(b-a)$, aspect ratio of the cavity (−)
K	thermal diffusivity of the fluid (m^2/s)
λ	thermal conductivity of the fluid (W/(m K))
ν	kinematic viscosity of the fluid (m^2/s)
Ω	Rotation rate of the inner cylinder (rad/s)
Φ	Heat flux supplied to the rotor (W/m^2)
*	denotes a normalized quantity
0	denotes a quantity evaluated at the inlet ($z=0$)
f	denotes a quantity evaluated in the fluid
P	denotes a quantity evaluated at the wall

cylinder and a cooled outer stationary one. They performed temperature measurements for a large range of parameters $Ta \leq 2\times10^6$ and $Re_Q \leq 5960$. In the turbulent regime, the Nusselt number is found to be independent of the Taylor number until the transition to the turbulent regime with vortices. Then, the Nusselt number becomes independent of the axial Reynolds number as the flow is dominated by rotation effects. More discussion about these four flow regimes may be found in the review of Fénot et al. [3].

Cornish [4] was the first to show that the length of the Taylor–Couette system has a preponderant effect on the transition to turbulence compared to the gap thickness. Becker and Kaye [2] showed that a longer cylindrical gap allows vortices to appear at lower Taylor numbers. Aoki et al. [5] performed a combined theoretical and experimental investigation of turbulent Taylor–Couette flows without any Poiseuille flow. Their most noticeable result is that the gap ratio $\Delta R/a$ in the range [0.055–0.132] has only a small effect on the heat transfer for three different fluids: air, iso-buthyl alcohol and spindle oil. They provided also numerous correlations for the Nusselt number according to the Taylor and Prandtl numbers. Ball et al. [6] showed experimentally that low radius ratios η tend to stabilize the flow (decrease in the local Taylor number) and so delay the appearance of Taylor vortices, which induce lower heat transfer coefficients. The influence of the aspect ratio Γ may be simply explained by a decreasing effect of input conditions when Γ is increased. Generally, the distance required for Taylor cells to appear increases with Re_Q and decreases with Ta. Kuzay and Scott [7] studied experimentally the turbulent heat transfer in the gap between an inner rotating or non rotating insulated cylinder and an outer stationary heated cylinder combined with an axial air flow. They established correlations for the Nusselt numbers against a new physical parameter, called the swirl parameter $N=\Omega a/\overline{V_z}$, which combines both the rotation and axial flow effects. Childs and Turner [8] showed that the Nusselt number along the rotor is a function of the axial Reynolds and Prandtl numbers to the power 0.8 and 0.5 respectively for $1.7\times10^5 \leq Re_Q \leq 13.7\times10^5$ and $6\times10^7 \leq Ta \leq 12\times10^{10}$ (Γ=13.3, η=0.869, in the case of an insulated stator and a heated rotor) in agreement with Kuzay and Scott [7], although they studied a very different configuration ($\Gamma=12$, $\eta=0.571$, insulated rotor and heated stator). Jakoby et al. [9] performed temperature measurements in the turbulent regime with vortices for $4000 \leq Re_Q \leq 30000$ and $Ta \leq 10^9$ and observed that the Nusselt number increases with Ta but remains independent of Re_Q. Gilchrist et al. [10] investigated the effect of surface roughness on the heat transfer for $10^6 \leq Ta \leq 5\times10^7$ and $900 \leq Re_Q \leq 2100$ using water as the working fluid. In the smooth case, the Nusselt number does not change with Re_Q. As expected, protusions on the inner cylinder enhance the heat transfer process. Tachinaba and Fukui [11] reported a transition in the Nusselt number distribution around $Ta \simeq 10^8$.

Escudier and Gouldson [12] performed velocity measurements by Laser Doppler Velocimetry (LDV) in a cavity characterized by $\Gamma=244$ and $\eta=0.506$ for various flow conditions and different fluids including Newtonian and shear-thinning fluids. For the Newtonian fluid in the turbulent regime, the radial distribution of the axial velocity and the pressure drop are similar to the ones observed in pipe flows. The radial distribution of the azimuthal velocity reveals a flow structure divided into three regions: two very thin boundary layers, one on each cylinder, separated by a central core in near solid body rotation. The main effect of the superimposed axial throughflow is to reduce the azimuthal velocity in the core region. Nouri and Whitelaw [13] measured the three mean velocity components and the associated Reynolds stress tensor of the flow subjected to an axial superimposed throughflow in a concentric annulus ($\Gamma=98$, $\eta=0.496$) with or without rotation of the inner cylinder. Compared to the non-rotating case, the rotation of the inner cylinder at $\Omega=300$ rpm does not affect the drag coefficient and the radial distribution of the mean axial velocity in the turbulent regime. It slightly enhances turbulence intensities especially close to the walls. For very large axial flowrates, there is absolutely no effect of the rotation of the inner shaft on both the mean axial flow and turbulence intensities. These two works provided very useful databases for future numerical benchmarks. One can cite for example the work of Kuosa et al. [14] who investigated the cooling of high-speed electrical machines, where only the inner cylinder is rotating. They compared the predictions of three different models: an algebraic modeling, a low-Reynolds number $k-\varepsilon$ modeling and a $k-\omega$ SST model. The hydrodynamic and thermal fields are established for various rotation rates and mass flowrates. The three turbulence models underestimated the entrainment coefficient of the fluid, which was attributed by the authors to the boundary conditions imposed at the inlet and outlet sections and to the turbulence models used. More recently, Friess et al. [15,16]

compared the predictions of Large-Eddy Simulation results obtained using the WALE model to the Elliptic Blending Reynolds Stress Model and a hybrid RANS/LES method both available within Code Saturne. As they considered the same radius ratio $\eta = 8/9$ and the same range of Ta and Re_Q values, their LES results for the hydrodynamic field will hold as reference data in the present paper. The main difference is that the flow is assumed to be periodic in the axial direction in the LES, simulating thus an infinite cavity. The flow is then hydrodynamically developed in their case, with the appearance of spiral networks within the boundary layers.

Recently, Fénot et al. [3] performed a very complete review on the heat transfer between concentric rotating cylinders with or without axial flow including smooth and slotted cavities. The actual state-of-art shows that the combined flow in such a system does not depend only on the global parameters such as the axial Reynolds and Taylor numbers, the geometry (η and Γ) but also on parietal thermal conditions, input hydrodynamic conditions … It explains partly that notwithstanding the abundant literature on that subject, there are still many open questions on the dynamics and heat transfer process and there is a need of an universal law to extrapolate the heat transfer for designing future rotating machineries. To get a global view of the state-of-art in this domain, the reader can also refer to the review by Maron and Cohen [17] or to the monograph of Childs [18].

The purpose of this work is to establish a new correlation for the Nusselt number along the rotor in the gap of an electrical machine schematized by a very narrow Taylor–Couette–Poiseuille system ($\Gamma = 50$, $\eta = 8/9$) for a large range of operating conditions and to discuss the heat transfer behavior having characterized in a first step the turbulent hydrodynamic field and the possible presence of coherent structures. The paper is organized as follows: the experimental set-up and measurement techniques are described in Section 2. The results about the hydrodynamic and thermal fields are discussed in details in Sections 3 and 4 respectively before some final conclusions in Section 5.

2. Experimental set-up and measurement techniques

2.1. General description and flow parameters

The system (Fig. 1a) is composed of two concentric vertical cylinders of length $h = 0.5$ m. The inner copper cylinder of radius $a = 8$ cm rotates around its axis at the rate Ω. The outer Plexiglas cylinder of radius $b = 9$ cm is stationary. The cavity is thus defined by an aspect ratio equal to $\Gamma = h/(b-a) = 50$ and a radius ratio equal to $\eta = a/b = 0.89$ (narrow gap cavity [19]). The outer cylinder is made of PMMA to allow optical velocimetry measurements. Both cylinders are located in a rectangular tank made also of PMMA that is regulated in temperature by a refrigerated circulator. The axial volumetric flow rate Q is imposed within the gap $\Delta R = b-a = 1$ cm by a centrifugal pump.

The main dynamic parameters characterizing such flows are the Taylor number Ta, defined as the ratio between centrifugal and viscous forces, and the axial Reynolds number Re_Q. The present definition of the Taylor number takes also into account possible geometrical variations through the hydraulic diameter $D_h = 2\Delta R$. Using water as the working fluid (instead of air for example) enables to consider weaker values of the rotation rate compared to real rotating machineries and thus allows tractable laboratory experiments to be realized. The Taylor and axial Reynolds numbers can be gathered to form the swirl parameter $N = \Omega a/\overline{V_z}$.

Before entering the rotor-stator cavity, the water flow coming from 6 pipes is collected in a small cavity. Then, water circulates from the top to the bottom of the cavity. When leaving the gap, water is gathered in an open tank, which is also regulated in temperature. Water temperature is measured at the entrance and at the outlet in the middle of the gap through a set of 2 PT 100 probes. The Prandtl number is fixed to $Pr = \nu/\kappa = 6$ (κ the thermal diffusivity of water) in most of the experiments but may be varied within the range [4.5–6] by changing the fluid temperature at the inlet.

2.2. Details about the rotor

The rotor, which is also dedicated to supply a maximum heat flux Φ of about 5.4 kW/m^2 to the fluid, is itself made of two concentric cylinders. The inner cylinder is a 6 cm radius aluminum tube. A 1 cm layer of cork was stuck on it to avoid heat losses. Then 60 m of a 4 mm diameter heating wire (1 Ω/m) was wound on the cork layer. Conductive silver paste was added to fill the gap between the rings. A 8 cm radius copper tube (5 mm thickness) was threaded on this assembly. In order to close the rotor, two PVC end caps (5 cm thick) were assembled on both sides. The motor shaft is

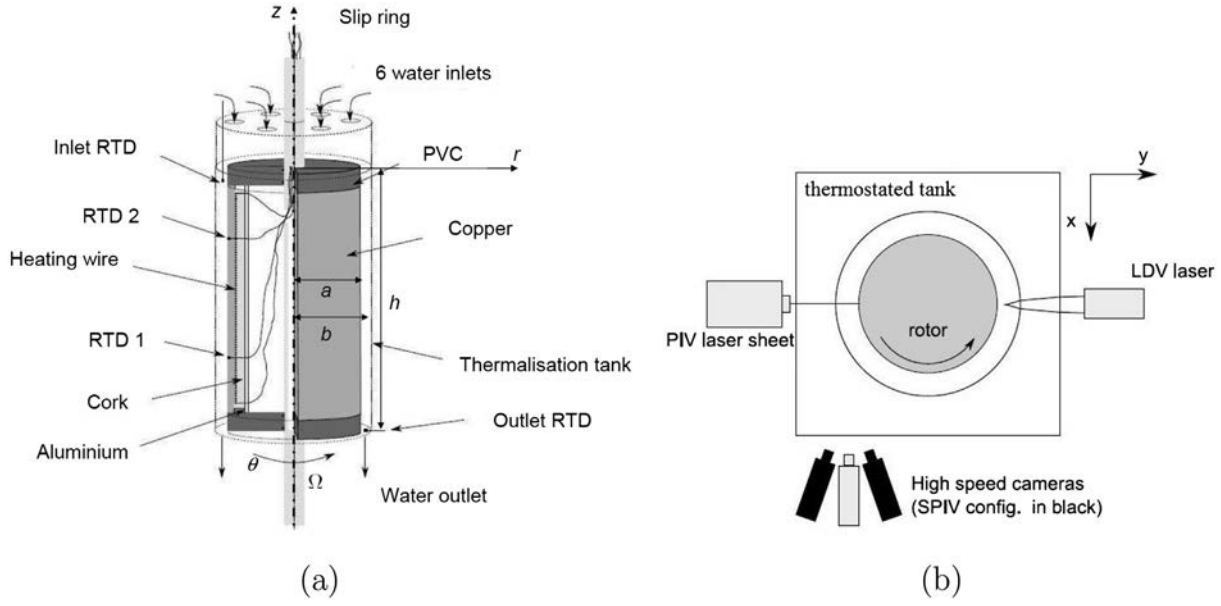

Fig. 1. (a) Schematic representation of the experimental facility and (b) top view of the different velocity measurement systems.

a 3 cm radius tube in stainless steel metal. A small hole was drilled in it to take out every wires (probes and heating resistance) from the inner part of the rotor to a slip ring located at the top of the shaft. The shaft was passed through the end caps of the rotor and sealing was achieved by two O-rings on both sides. Pressure screws on the end caps allow a proper alignment (±0.15 mm) and positioning of the cylinders respectively to the shaft. The rotor is mounted on 2 bearings.

To perform parietal temperature measurements, 4 RTD probes (PT100) were mounted flush on the outer surface of the rotor. They were arranged in two diametrically opposite pairs located at 16.7 and 33.3 cm from the top of the cylinder. Data were acquired using a 4 channel analog module. These 4 probes provide the same values as a calibrated probe within 0.6%. The same measurements have been repeated several times and the maximum difference on the temperature measurements is 5.8×10^{-4} K.

2.3. Experimental procedure and data treatment

The axial and azimuthal components of the velocity vector are measured by a two-component LDV system arranged as shown in Fig. 1b. Seeding is achieved with 5 μm polyamide particles. Each run is conducted during 2 min in order to obtain a statistical convergence of the velocity. The error margins are ±3% and ±5% for the first and second-order momentums respectively.

PIV and SPIV (Stereo-PIV) measurements are also performed by using a 5 W continuous laser and two high speed cameras. Data acquisition frequency is set at 1500 Hz for a 512 × 1024 pixels resolution. The camera buffer limits the acquisition time to 2.6 s. For PIV measurements, polyamide particles of 30 μm in diameter are used to seed the flow. Cross-correlations between the different frames are performed with the software DPIVSoft [20]. First interrogation windows are composed of 64 × 64 pixels with 50% overlapping. They are then translated and deformed according to the velocity field estimation. Smaller windows (32 × 32 pixels with 50% overlapping) are then chosen to enhance the spatial resolution. LDV and PIV measurements have been favorably compared in terms of velocity and turbulent intensities in Aubert et al. [21].

The experimental procedure for the temperature measurements is described as follows. At first, the different temperature regulation systems are switched on. The pump is also turned on and the gap is filled with water before starting the rotation of the inner cylinder. As the temperature of the outer rectangular tank is regulated at the temperature of the working fluid flowing between the two cylinders, there is no heat flux through the stationary cylinder. When the whole system reaches the thermal equilibrium, data acquisition is triggered. Finally, the heating wire is powered. Around 2 h and a half are necessary for the system to reach the steady state. The temperature of the incoming fluid is then close to 25 °C. A 2D axisymmetric model developed with COMSOL allowed to estimate the heat loss in the system considering conductive transfers through the shaft. The wall heat flux is found to be equal to 90% of the flux provided by the heating wire.

3. Transitional or developed flow regime?

The minimum values for the flow parameters considered here are: $Ta = 8.8 \times 10^6$ and $Re_Q = 7490$. According to the diagram established by Becker and Kaye [2] for longer cavities, one should expect to obtain a turbulent flow regime without any Taylor vortices. In the following, all quantities are shown in their dimensionless form: the radial $r^* = (r-a)/(b-a)$ and axial $z^* = z/h$ coordinates, the mean tangential $V_\theta^* = V_\theta/(\Omega a)$ and axial $V_z^* = V_z/\overline{V_z}$ velocity components and the corresponding normal components $R_{\theta\theta}^* = \overline{v_\theta'^2}/(\Omega a)^2$ and $R_{zz}^* = \overline{v_z'^2}/\overline{V_z}^2$ of the Reynolds stress tensor.

3.1. Mean velocity profiles

Velocity measurements have been performed here using a two-component LDV system and compared to the LES results of Friess et al. [15,16] for a periodic cavity. As the cavity length h is only equal to 25 times the hydraulic diameter D_h, one could expect that for all sets of parameters (Ta, Re_a), the cavity is too short to permit a well developed flow. The aim of this section is to check this fact for various flow conditions and to possibly explain the variations of the Nusselt number with (Ta, Re_Q) in the next section.

The influence of the flow parameters (Ta, Re_Q) on the mean flow field is now investigated. The LDV measurements are plotted at $z^* = 0.9$ (22.5 D_h) in terms of two mean velocity components V_θ^* and V_z^* for two axial Reynolds numbers and three Taylor numbers (Fig. 2). Because of technical constraints (laser reflection, wall curvature and seeding of particles), measurements are made difficult close to the walls.

The radial distributions of the mean tangential velocity presented in Fig. 2a and b clearly show a flow divided into 3 regions: two boundary layers developed on each cylinder and a central region. The $V_\theta-$ profile is almost constant in this region when rotation effects are dominant, which is the case when the swirl parameter is large enough: $N = 6.71$ for $Ta = 7.9 \times 10^7$ and $Re_Q = 7490$. For smaller values of N, increasing the axial flow (or Re_Q) or decreasing the rotation rate of the inner cylinder (or Ta) induces a slope in the profile. Thus, V_θ^* varies linearly with $1/r$ within the gap such that the angular momentum is conserved. Decreasing the swirl parameter N also induces a decrease in the mean tangential velocity around mid-gap. For example, $V_\theta^* \simeq 0.2$ at $r^* \simeq 0.5$ for $N = 1.49$ ($Ta = 8.8 \times 10^6$, $Re_Q = 11{,}200$) far from the value $V_\theta^* \simeq 0.5$ obtained by the LES of Friess et al. [15,16] for a fully developed flow. It means that for this value of the swirl number, the hydrodynamic field is not developed in the experiment even for $z^* = 0.9$ ($=22.5 D_h$).

In the experiments, the radial distribution of the mean axial velocity component (Fig. 2c and d) resembles a turbulent Poiseuille profile typically encountered in turbulent pipe flows. A large asymmetry is observed for the highest value of the axial Reynolds number $Re_Q = 11{,}200$ with a more intense axial flow along the outer cylinder. This comforts the fact that it is difficult to increase easily heat transfers through the boundary layers of rotating devices when blowing on them: longitudinal flows seems to be expelled from these rotating layers. Apart from this asymmetry, the effects of both the Taylor and axial Reynolds numbers remain weak and the experimental data are in good qualitative agreement with the LES of Friess et al. [15,16] for the same sets of parameters but for a periodic axial flow.

3.2. Turbulent field

Gollub and Swinney [22] have shown experimentally that the flow transits to turbulence for $Ta/Ta_c \simeq 1300$, which was confirmed numerically by Alziary de Rocquefort and Grillaud [23]. Ta_c is the critical Taylor number for the transition to the Taylor vortex regime depending on the radius ratio η. Thus, for $\eta = 8/9$, $Ta_c \simeq 2500$ after Cognet [24]. One can thus expect to observe a turbulent regime for $Ta \geq 3.25 \times 10^6$.

Fig. 3 highlights the influence of the parameters on the turbulent field. As expected, higher values of the Taylor number induce higher turbulence levels within the gap and in the boundary layers whatever the value of Re_Q. This result is not so intuitive for the azimuthal normal component due to the normalization by $(\Omega a)^2$. It means that the azimuthal turbulence intensities increase more rapidly than the rotation rate of the inner cylinder, which cannot be attributed to the axial flowrate fixed at a constant value. The experimental trends are quite similar to those obtained

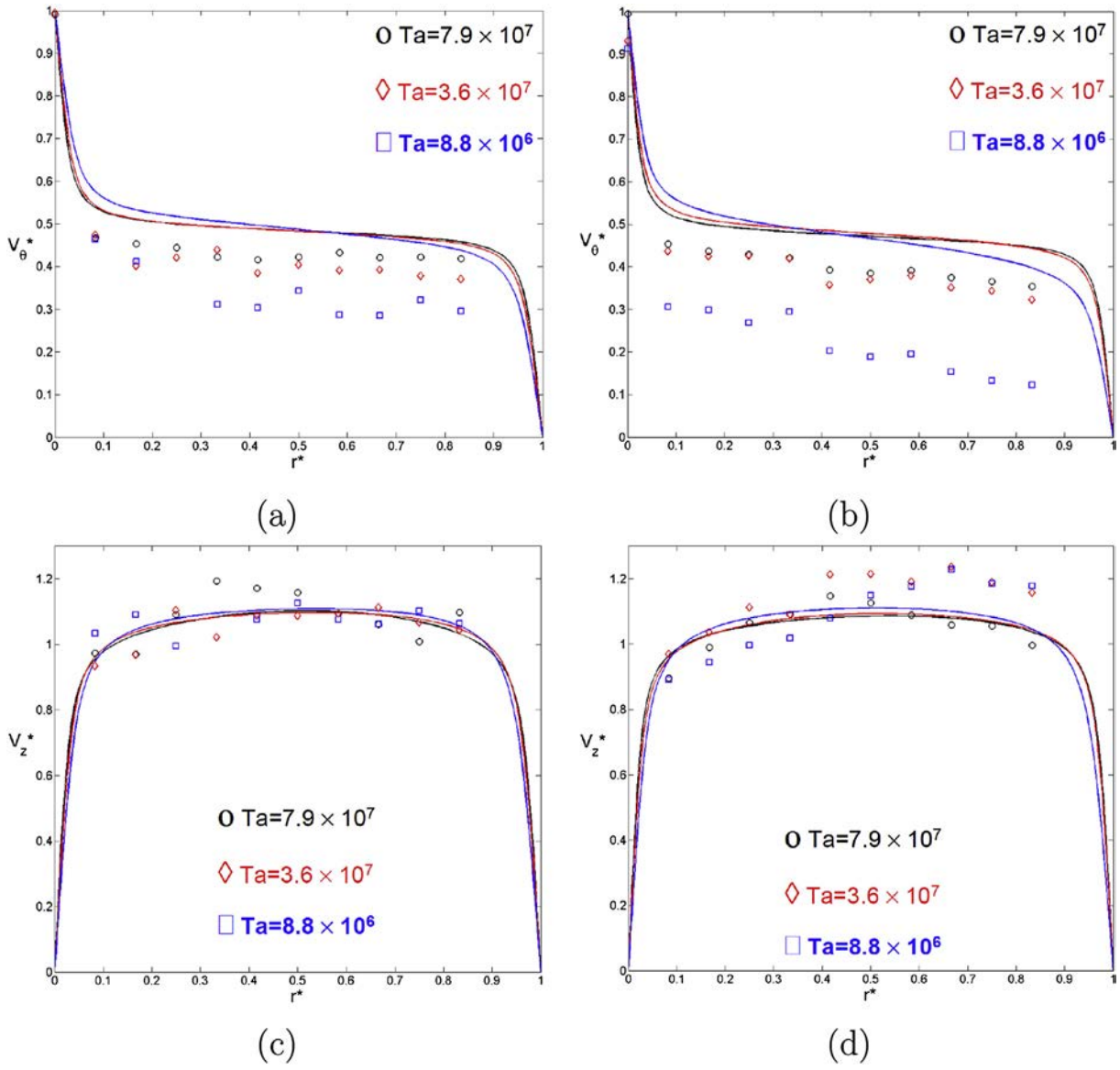

Fig. 2. Influence of the Taylor number on the mean (a, b) azimuthal V_θ^* and (c, d) axial V_z^* velocity components for $Re_Q = 7490$ (a, c) and $Re_Q = 11{,}200$ (b, d). Comparison between the present LDV measurements (symbols) obtained at $z^* = 0.9$ and the LES results (lines) of Friess et al. [15,16] obtained in a periodic cavity.

numerically by Friess et al. [15,16] with higher intensities when one moves towards the boundary layers attached to the walls. The LDV measurements seem to be less sensitive to the rotation rate. By comparisons between Fig. 3a–d, it can be seen that the effect of the axial flowrate remains weak. It is also noticeable here that the intensities of the Reynolds stress tensor observed experimentally within the gap are remarkably high compared to those published in previous papers [13,25,26]. As it will be seen in the next paragraph, this can be explained by the presence of active coherent structures located in the near-wall regions.

3.3. Coherent structures

The appearance of coherent vortices within the boundary layers is crucial to predict accurately the heat transfer coefficients and better understand its behaviors. Heat transfer is generally enhanced by the appearance of such vortices when the Taylor number is increased. In particular, this could explain why most of the RANS models, which assume the base flow as being stationary and axisymmetric, fail to predict the right distributions of the heat transfer coefficient [27].

To explore the possible existence of spiral networks within the boundary layers as obtained in a periodic cavity by Friess et al. [15,16], SPIV measurements have been performed at a sufficiently high frequency (1500 Hz) to be resolved in time and to make the Taylor hypothesis valid. By considering also that the flow has mainly constant azimuthal velocity radial profile, one can calculate the λ_2 criterion, which is the second eigenvalue of the $S^2 + A^2$ tensor, where S and A are the symmetric and antisymmetric parts of the velocity gradient tensor approximated using second-order finite-difference schemes. The iso-values of λ_2 enable to highlight the presence of coherent structures within the flow. One example is given in Fig. 4 for $Re_Q = 7490$ and $Ta = 8.7 \times v10^6$. The axial fluid flows from the top to the bottom and time is increasing from the right to the left. Coherent structures along the rotor side can be observed with a negative inclination angle, suggesting a qualitative good agreement with the iso-values of the Q criterion obtained numerically by Friess et al. [15,16]. Fig. 4 shows also that there is no

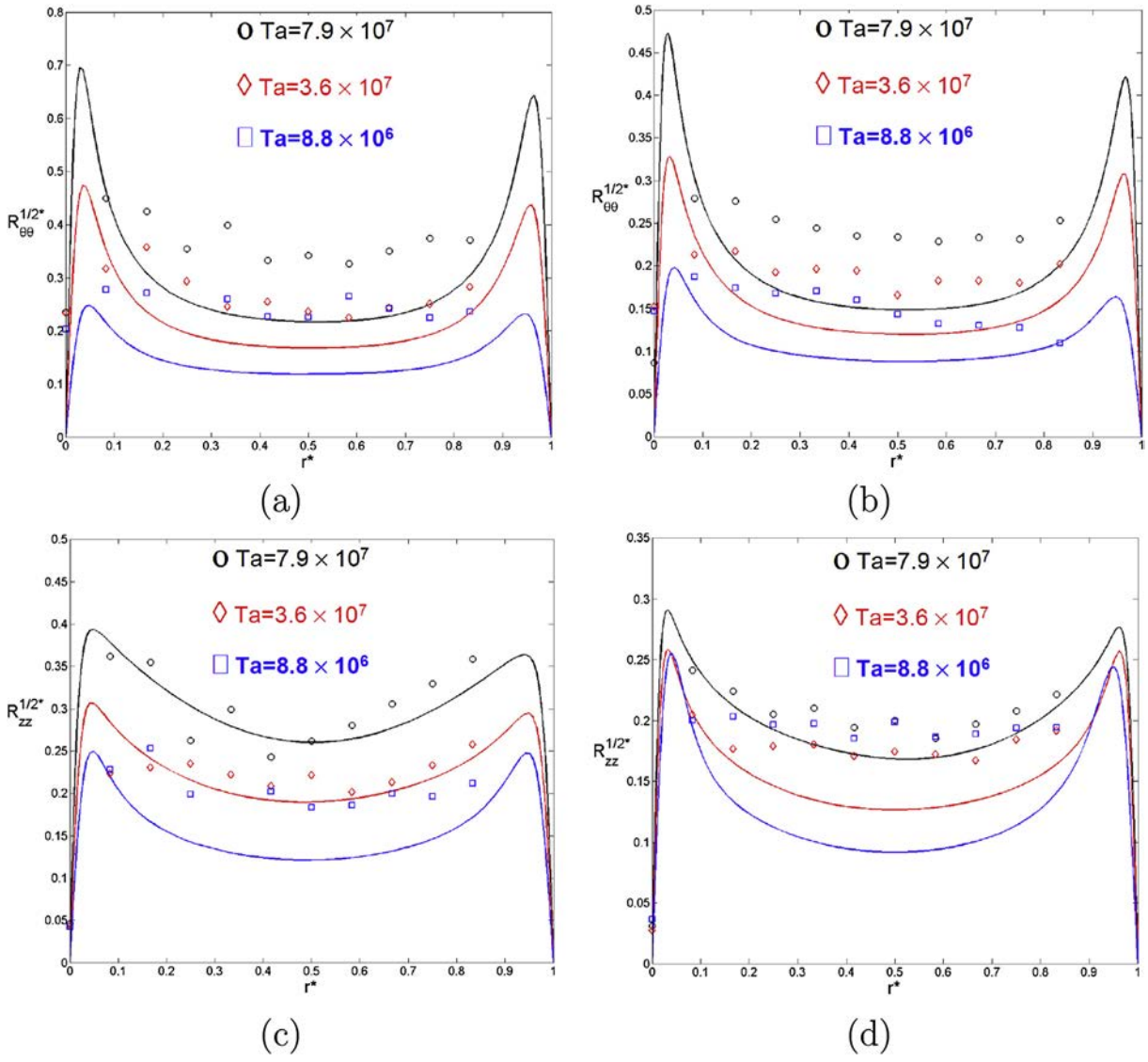

Fig. 3. Influence of the Taylor number on the normal components (a, b) $R_{\theta\theta}^{*1/2}$ and (c, d) $R_{zz}^{*1/2}$ for $Re_Q = 7490$ (a, c) and $Re_Q = 11{,}200$ (b, d). Comparison between the present LDV measurements (symbols) obtained at $z^* = 0.9$ and the LES results (lines) of Friess et al. [15,16] obtained in a periodic cavity.

apparent 3*D* large scale vortices within the core of the flow. A similar experiment performed at $Re_Q = 7490$ and $Ta = 7.9 \times 10^7$ showed the same flow structure except that the inclination angle is smaller.

4. Heat transfer distribution along the rotor

From an engineering point of view, the main goal of this section is to establish correlations for the heat transfer coefficient on the rotor wall according to the flow parameters: Re_Q, Ta and the Prandtl number Pr. An analytical model based on the former work of Aoki et al. [5] has been first developed for turbulent flows and then compared to extensive temperature measurements.

4.1. Analytical model for the heat transfer coefficient

Aoki et al. [5] developed an analytical model to predict the Nusselt number on the rotor side for laminar Taylor–Couette flows. This model has been extended here to the turbulent regime. If one assumes that the flow may be divided into two flow regions, the inviscid region where the mixing effect of disturbance is very large and the viscous dominant region near the wall, the classical boundary layer theory in the turbulent regime gives the following relation:

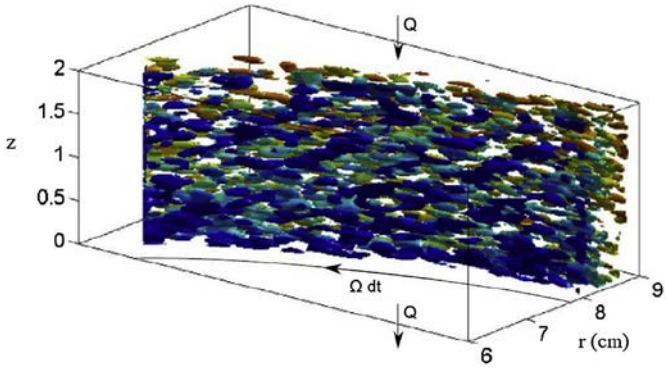

Fig. 4. Iso-values of the λ_2 criterion ($\lambda_2 = 10^3$) obtained experimentally from SPIV measurements for $Re_Q = 7490$ and $Ta = 8.7 \times 10^6$.

$$\frac{\delta}{\Delta R} \sim \left(\frac{V_{eff}\,\Delta R}{\nu}\right)^{-1/5} \tag{1}$$

where V_{eff} represents the velocity at the boundary of the two regions. The balance between the centrifugal and viscous forces in the boundary layer region is:

$$\Omega^2 a \sim \frac{V_{eff}\,\nu}{\delta^2} \tag{2}$$

Then, the expression for $\delta/\Delta R$ representing the velocity gradient at the wall gets:

$$\frac{\delta}{\Delta R} \sim \left(\frac{\Omega^2 a \Delta R^3}{\nu^2}\right)^{-1/7} \tag{3}$$

As the heat transfer is purely conductive within the boundary layer, $h = \lambda/\delta$. One finally obtains:

$$Nu = \frac{h\Delta R}{\lambda} \sim Ta^{1/7} \tag{4}$$

The power 1/7 is quite low and shows that the heat transfers are controlled and thus limited by the decrease of δ versus Ω. The rotor is wrapped in a conductive jacket. This quite intuitive simple model explain the difficulties met by engineers to cool down the rotors of electric motors for instance. It is also worth to note that if one changes abruptly by a tiny amount the rotation speed of the rotating cylinder (touching it with the hand for instance), it is quite easy to dramatically increase the Nusselt number as the rotating boundary layer will be peeled off by the shear caused by differential rotation.

4.2. Correlation for the Nusselt number along the rotor wall

Fig. 5 shows the evolution of the Nusselt number *Nu* measured at two axial positions along the rotor as a function of the Taylor number for various axial Reynolds numbers Re_Q. There is a noticeable difference between the values obtained by the two probes (at $z^* = 0.32$ and 0.66). This difference comes from the transient nature of the flow and as a consequence of the heat transfer process (see in Ref. [28]). *Nu* is clearly an increasing function of *Ta* with more important variations for weak rotation rates. It may be attributed to the coherent structures observed within the rotor boundary layer, which would prevent the axial flow to cool the rotor at high rotation rates. The same tendency is obtained whatever the axial Reynolds number Re_Q, whose effect is to increase the heat transfer coefficient at a given Taylor number. The present measurements are in good agreement with the experimental data of Gilchrist et al. [10] obtained using water at 60° for $\Gamma = 107$, $\eta = 0.83$, $950 \leq Re_Q \leq 2080$ and within the same range of Taylor numbers.

The experimental data plotted in Fig. 5 have also been fitted by correlation laws under the form: $Nu = B\Delta R(\Omega/\nu)^{2/7}$, with *B* an adjusting coefficient equal to 26 for the probe at $z^* = 0.32$ and Re_Q= 11,200 as example. It is based on both the boundary theory in the turbulent regime and the assumption that heat transfer is purely conductive. It works quite well especially for $Ta > 2 \times 10^7$. It confirms, in particular, that the Nusselt number depends on the Taylor number with an exponent close to 1/7 ($\simeq$0.144) as found by Equation (4), whereas Gilchrist et al. [10] found an exponent equal to 0.226. This difference may be explained by the fact that these authors considered a much higher aspect ratio (enabling to expect a fully developed flow in the axial direction) and a narrower range of *Ta* values and by the fact that their correlation is obtained for the averaged Nusselt number along the whole inner cylinder inducing higher values due to edge effects.

As sometime met in the literature [3], one can also try to gather the results and express the Nusselt number under the form:

$$Nu = A\mathrm{Re}_{eff}^{\beta} \tag{5}$$

where $Re_{eff} = (V_{eff} \times D_h)/\nu$ is an effective Reynolds number based on an effective velocity $V_{eff} = (\overline{V_z}^2 + \alpha(\Omega a)^2)^{1/2}$ taking into account both the axial flow and rotation effects. The coefficient α represents the relative importance of rotation compared to the axial flowrate. It is usually arbitrarily fixed to 0.5 (see in Ref. [3]). Fig. 6 shows the evolution of *Nu* against Re_{eff} for $\alpha = 0.5$ and various sets of parameters (*Ta*, Re_Q). As can be seen on the figure, the experimental results are well scaled by a linear interpolation with $A = 0.92$ and $\beta = 0.27$. Note however that, in the present case, the coefficient

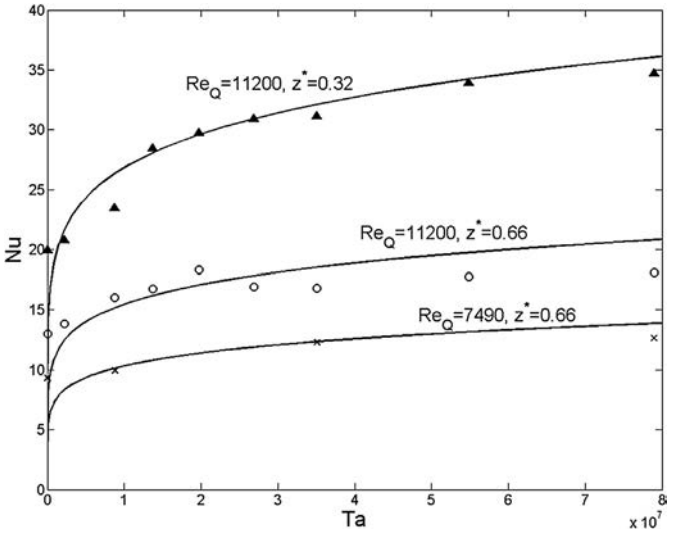

Fig. 5. Evolution of the Nusselt number according to the Taylor number for various axial Reynolds numbers. The lines correspond to the scalings deduced from Equation (4).

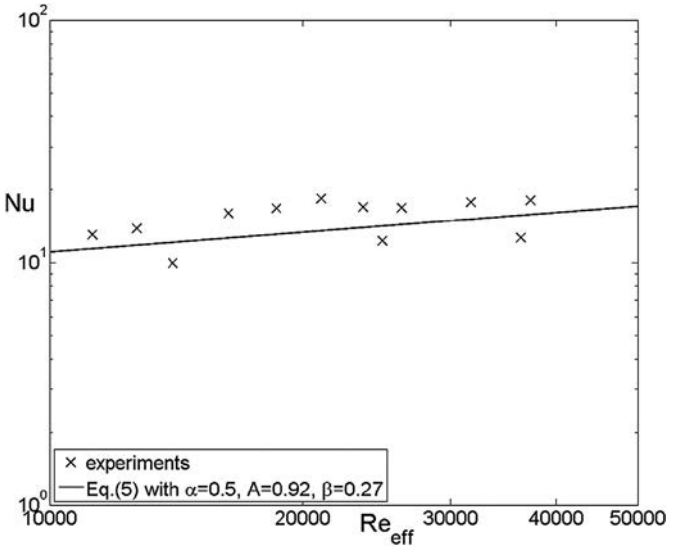

Fig. 6. Evolution of the Nusselt number *Nu* at $z^* = 0.66$ according to the effective Reynolds number Re_{eff}. Comparisons between the experiments for $Pr = 6$ and the linear interpolation (Equation (5)) obtained using $\alpha = 0.5$, $A = 0.92$ and $\beta = 0.27$.

$\beta = 0.27$ is relatively far from all previous studies that report β in the range [0.7–0.8] for Taylor–Couette–Poiseuille flows [3] or encountered in many duct correlations.

To go a little further and in particular to take into account the Prandtl number dependence of the heat exchanges, a set of experiments has been performed where the thermalization of the working fluid (and of the outer rectangular tank) is removed. The water temperature can therefore drift slowly from the steady state and the Prandtl number as well in the range [4.5–6]. Note that due to temperature change, Re_Q and Ta are also modified. These experiments have been done for four sets of parameters in the range $7490 < Re_Q < 11{,}200$ and $8.8 \times 10^6 < Ta < 7.9 \times 10^7$ such that, $4 \times 15{,}000$ measurements have been analyzed. Attempts to find a correlation for the Nusselt number under the form $Nu = ARe_{eff}^{\beta} Pr^{\gamma}$ or $Nu = Re_Q^{\alpha} Ta^{\beta} Pr^{\gamma}$ were not successful. This may come from the small range of variations for the Prandtl number. However as Re_Q and Ta were also changing with the temperature, these experiments still represent a huge source of information to look for a correlation giving the Nusselt number distribution. This is why in the following the exponent for the Prandtl number is assumed to be equal to the classical value 1/3. Thus, this time, the experimental data may be correlated under the form:

$$Nu\mathrm{Pr}^{-1/3} = A\mathrm{Re}_{eff}^{\beta} \tag{6}$$

Using the method of least squares, the coefficients A, β can be deduced for different values of α used in the literature [3] (see Table 1). The usual value for β found in the literature is 0.8 far from the one obtained here around 0.5. Finally, a third correlation can been calculated using an error minimization by the least square method over the same $4 \times 15{,}000$ measurements and using the preceding parameter Re_Q and forcing as before the exponent of the Prandtl number equal to 1/3. It provides the final correlation law for Nu at $z^* = 0.66$:

$$Nu = 6.137 \times 10^{-4} \mathrm{Re}_Q^{0.77} Ta^{0.127} \mathrm{Pr}^{1/3} \tag{7}$$

It confirms, in particular, that the Nusselt number depends on the Taylor number with an exponent close to 1/7 as found by Equation (4). Tachibana and Fukui [11] and Tzeng [29], who were the only ones to work at such high Taylor numbers (up to 10^8) recorded an exponent close to 1/3 and 1/4 respectively. Tzeng [29] attributed its much higher heat transfer to the presence of Taylor vortices. One can cite also Becker and Kayer [2], who reported an exponent equal to 0.241 at high Taylor numbers (see in Ref. [3] for more correlations). The exponent for the axial Reynolds number 0.77 is in very good agreement with the classical one found in the literature 0.8 [18]. The experimental values of the Nusselt number Nu evaluated at $z^* = 0.66$ for the experiments in steady state (Fig. 5) are plotted against the Equation (7) obtained through the temperature drift experiments in Fig. 7. As can be seen on the figure, the agreement is quite good except for the 3 first data points for which the Nusselt number is higher than its predicted values. These measurements correspond in fact to the lower values of the Taylor and axial Reynolds number flows, values that are not in the range for which the correlation was developed. Thus it is quite understandable that these three points escape from the general turbulent description.

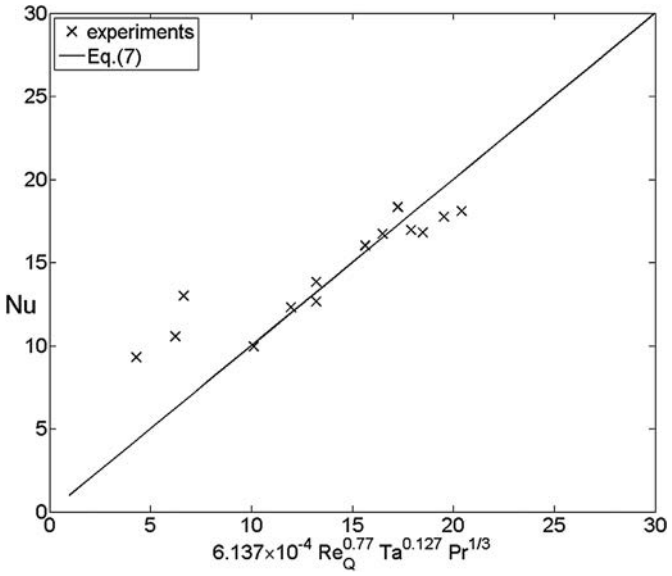

Fig. 7. Local Nusselt numbers evaluated at $z^* = 0.66$ for the experiments performed in steady state (cf Fig. 5) plotted against the correlation given by Equation (7) obtained through the temperature drift experiments.

The experimental data for the Nusselt number have been also compared to the predictions of the Reynolds Stress Model available within Fluent in its low Reynolds number formulation for $Pr = 6$, $Re_Q = 11200$ and three Taylor numbers (Table 2). Calculations are steady axisymmetric with (81×500) mesh points in the radial and axial directions respectively. The geometrical parameters of the cavity are strictly the same as in the experiments. The Reynolds and energy equations are coupled through the Boussinesq approximation without the viscous dissipation term. It has been checked that the inlet boundary conditions (turbulence intensities, velocity profiles) have only a weak influence on the velocity profiles and on the Nusselt distributions. Thus, the input conditions are a turbulent Poiseuille profile for the axial velocity component with a turbulence level equal to 1%. The LES results of Friess et al. [15,16] have also been extented to non-isothermal flows by Poncet [28] still assuming a periodic flow in the axial direction. The results of Poncet [28] are also provided for comparisons in Table 2.

One can notice first a large discrepancy between the different approaches, with an overestimation of the Nusselt number by the numerics. There is no apparent reason, which could explain such a large overestimation by the RSM (Fluent) compared to the experiment, as the same boundary conditions and flow parameters have been considered. In their review paper, Fénot et al. [3] attributed the disparities in the reported results by the fact that input

Table 1
Experimental values of the coefficients A, β and γ used in Equation (6) for different values of α.

	η	Γ	Re_Q	Ta	Experimental conditions	α	A	β
Present experiments	8/9	50	1.12×10^4	7.9×10^7	Insulated stator, heated rotor	0.25	0.03	0.54
Present experiments	8/9	50	1.12×10^4	7.9×10^7	Insulated stator, heated rotor	0.5	0.05	0.48
Bouafia et al. [31].	0.956	98.4	1.1×10^4–3.1×10^4	1800–4×10^6	Cooled stator, heated rotor	0.5	0.025	0.8
Present experiments	8/9	50	1.12×10^4	7.9×10^7	Insulated stator, heated rotor	0.6	0.06	0.47
Kosterin and Finat'ev [32].	0.78	77.5	3×10^4–3×10^5	$\leq 8 \times 10^5$	Insulated stator, heated rotor	0.6	0.018	0.8
Present experiments	8/9	50	1.12×10^4	7.9×10^7	Insulated stator, heated rotor	0.8	0.06	0.46
Grosgeorge [33].	0.98	200	9900–26850	1.4×10^5–4.9×10^6	Insulated stator, heated rotor	0.8	$f(Re_Q)$	0.8

Table 2
Values of the Nusselt number at $z^* = 0.66$ for various flow parameters. Comparisons between the experimental data, the RSM (Fluent) and the LES results of Poncet [28].

Ta	Re_Q	$Pr = 6$
8.8×10^6	11,200	16.01 (exp.)
		73.4 (RSM)
		19.25 (LES [28])
3.5×10^7	11,200	16.81 (exp.)
		125.4 (RSM)
		51.6 (LES [28])
7.9×10^7	11,200	18.09 (exp.)
		156.3 (RSM)
		64.65 (LES [28])

conditions for the thermal and hydrodynamic fields are generally not taken into account. Changing the turbulence intensities at the inlet or the type of velocity profiles does not modify significantly the averaged value for the Nusselt number on the rotor. For example, Nu is 15% lower if the turbulence intensities imposed at the inlet decrease from 10% to 1%, which is not enough to explain the difference with the experiments. It may be attributed to both the presence of 3D structures within the boundary layers not captured by the RSM (Fluent) and to the turbulence modeling, which is not adapted to confined rotating flows with heat transfer. The overestimation by the LES of [28] may be fully explained by the presence of the spiral vortices due to the axial periodicity of the flow. These structures greatly favor the heat transfer process in the numerics as also observed by Hirai et al. [30], who reported a very sharp increase of Nu when the coherent vortices appear.

4.3. Viscous dissipation

The measure of the heat source by viscous dissipation has also been performed in the experiment with no axial flow and for both fluids: water and air. For a water flow at a Taylor number equal to 7.9×10^7, an increase of 0.085 K per hour has been registered. For an air flow at the same Ta, one has estimated the dissipated power being equal to 0.26 W, which would correspond to an increase in temperature of 300 K per hour. This last value is, of course, not negligible but one recalls that no axial flow is here imposed. The power injected in the fluid by viscous dissipation remains weak in all cases except for long time experiments using air as the working fluid. Nevertheless, when an axial flow is imposed, the increase in temperature is much lower. By supposing that the dissipated power due to viscosity remains the same (denoted here P_{inj}), one can also estimate the increase in temperature ΔT as a function of the axial mass flowrate q_m: $\Delta T = P_{inj}/(c_p q_m)$. Thus, for a flowrate equal to 0.01 m^3/s, the increase in ΔT is reduced to 79.2 K per hour. The influence of the viscous dissipation term on the Nusselt number has been also checked numerically using the RSM model of Fluent. For $Pr = 6$, $Re_Q = 7490$ and $Ta = 7.8 \times 10^7$, the Nusselt number is slightly lower with the viscous dissipation term. The maximum difference is 1.25 at a given axial position, such that the difference is less than 1% on the mean value. Thus, this term is not preponderant in the present case.

5. Conclusion

In this paper, turbulent non-isothermal flows between two concentric cylinders, where only the inner cylinder is rotating, have been considered experimentally for an open cavity characterized by an aspect ratio $\Gamma = 50$ and a radius ratio $\eta = 8/9$. Velocity and temperature measurements have been performed. The influence of the flow parameters (Taylor $Ta \leq 7.9 \times 10^7$ and axial Reynolds $Re_Q \leq 11{,}200$ numbers) has been discussed in details.

As it is always the case in engineering installations, the hydrodynamic field is not fully established at the cavity outlet in the experiment depending on the operating conditions. Turbulence levels are remarkably high within the gap and especially in the very thin boundary layers, which developed along both walls. SPIV measurements highlighted also the presence of coherent structures along both walls.

A correlation for the rotor Nusselt number measured at $z^* = 0.66$ has been established from the analyses of 60,000 measurements. On the rotor side, the Nusselt number depends on the axial Reynolds number Re_Q to the power 0.77, on the Taylor number Ta to the power ~0.13 when the Prandtl number dependence with a power 1/3 is imposed. Therefore the exponent for the Taylor number confirms the value 1/7 predicted analytically from the turbulent boundary layer theory. The present model and experimental data confirm the fact that heat transfers are essentially controlled by the thickness of the rotating viscous layer attached to the rotor whatever the rate of the axial throughflow is. This explains the difficulty met by engineers to cool down rotating shafts of industrial apparatus by blowing a longitudinal flow on them.

One has also illustrated the difficulty of numerical simulations to reproduce the exact heat transfers levels as these are controlled by thin layers or sometimes coherent structures confined near the walls. LES calculations in a finite cavity are now required to confirm the present experimental results, provide more information about the turbulence structures within the boundary layers and cover also a wider range of the flow parameters and especially to simulate air flows.

Acknowledgment

The authors would like to thank Liebherr Aerospace Toulouse Grant 300 17596 for their financial support as well as the LABEX MEC (ANR-11-LABX-0092) through the HYDREX program.

References

[1] J. Kaye, E.C. Elgar, Modes of adiabatic and diabatic fluid flow in an annulus with an inner rotating cylinder, Trans. ASME J. Heat Transfer 80 (1958) 753–765.
[2] K.M. Becker, J. Kaye, Measurement of diabatic flow in an annulus with an inner rotating cylinder, Trans. ASME J Heat Transfer 84 (1962) 97–105.
[3] M. Fénot, Y. Bertin, E. Dorignac, G. Lalizel, A review of heat transfer between concentric rotating cylinders with or without axial flow, Int. J. Therm. Sci. 50 (7) (2011) 1138–1155.
[4] R.J. Cornish, Flow of water through fine clearances with relative motion of the boundaries, Proc. R. Soc. Lond. Ser. A 140 (1933) 227–240.
[5] H. Aoki, H. Nohira, H. Arai, Convective heat transfer in an annulus with an inner rotating cylinder, Bull. JSME 10 (39) (1967) 523–532.
[6] K.S. Ball, B. Farouk, V.C. Dixit, An experimental study of heat transfer in a vertical annulus with a rotating inner cylinder, Int. J. Heat Mass Transfer 32 (1989) 1517–1527.
[7] T.M. Kuzay, C.J. Scott, Turbulent heat transfer studies in annulus with inner cylinder rotation, J. Heat Transfer 99 (1977) 12–19.
[8] P.R.N. Childs, A.B. Turner, Heat transfer on the surface of a cylinder rotating in an annulus at high axial and rotational Reynolds numbers, in: 10th Int. Heat Transfer Conference, 1994, pp. 13–18. Brighton.
[9] R. Jakoby, S. Kim, S. Wittig, Correlations of the convective heat transfer in annular channels with rotating inner cylinder, J. Eng. Gas Turbines Power 121 (4) (1999) 670–677.
[10] S. Gilchrist, C.Y. Ching, D. Ewing, Heat transfer enhancement in axial Taylor–Couette flow, in: Proc. ASME Summer Heat Conference, vol. 1, 2005, pp. 227–233. San Francisco.
[11] F. Tachibana, S. Fukui, Convective heat transfer of the rotational and axial flow between concentric cylinders, Bull. JSME 7 (26) (1964) 385–391.
[12] M.P. Escudier, I.W. Gouldson, Concentric annular flow with centerbody rotation of a Newtonian and a shear-thinning liquid, Int. J. Heat Fluid Flow 16 (1995) 156–162.
[13] J.M. Nouri, J.H. Whitelaw, Flow of Newtonian and non-Newtonian fluids in a concentric annulus with rotation of the inner cylinder, J. Fluid Eng. 116 (1994) 821–827.

[14] M. Kuosa, P. Sallinen, J. Larjola, Numerical and experimental modelling of gas flow and heat transfer in the air gap of an electric machine, J. Therm. Sci. 13 (3) (2004) 264–278.
[15] C. Friess, S. Poncet, S. Viazzo, Taylor-Couette-Poiseuille Flows: from RANS to LES, in: Int. Symp. Turb. Shear Flow Phenomena, TSFP8, Poitiers, 2013.
[16] C. Friess, S. Poncet, S. Viazzo, An extensive study on LES, RANS and hybrid RANS/LES simulation of a narrow-gap open Taylor–Couette flow, in: ASME 4th Joint US-European Fluids Engineering Summer Meeting, Chicago, 2014.
[17] D.M. Maron, S. Cohen, Hydrodynamics and heat/mass transfer near rotating surfaces, Adv. Heat Transfer 21 (1992) 141–180.
[18] P.R.N. Childs, Rotating Flow, Butterworth-Heinemann, Oxford, 2011.
[19] M. Biage, J.C.C. Campos, Visualization study and quantitative velocity measurements in turbulent Taylor–Couette flow tagging: a description of the transition to turbulence, J. Braz. Soc. Mech. Sci. Eng. 25 (4) (2003) 378–390.
[20] P. Meunier, T. Leweke, Analysis and minimization of errors due to high gradients in particle image velocimetry, Exp. Fluids 35 (2003) 408–421.
[21] A. Aubert, S. Poncet, P. Le Gal, S. Viazzo, M. Le Bars, T. Thouveny, Heat and mass transfer in turbulent Taylor–Couette flows with an axial throughflow, in: 21e Congrès Français de Mécanique, Bordeaux, 2013.
[22] J.P. Gollub, H.L. Swinney, Onset of turbulence in a rotating fluid, Phys. Rev. Lett. 35 (1975) 927–930.
[23] T. Alziary de Rocquefort, G. Grillaud, Computation of Taylor vortex flow by a transient implicit method, Comput. Fluids 6 (4) (1978) 256–269.
[24] G. Cognet, Les étapes vers la turbulence dans l'écoulement de Couette–Taylor entre cylindres coaxiaux, J. Mécanique Théorique Appliquée (1984) 7–44.
[25] S.Y. Chung, H.J. Sung, Large-eddy simulation of turbulent flow in a concentric annulus with rotation of an inner cylinder, Int. J. Heat Fluid Flow 26 (2005) 191–203.
[26] S. Poncet, S. Haddadi, S. Viazzo, Numerical modeling of fluid flow and heat transfer in a narrow Taylor–Couette-Poiseuille system, Int. J. Heat Fluid Flow 32 (2011) 128–144.
[27] J.M. Owen, Flow and heat transfer in rotating disc systems, in: Y. Nagano, K. Hanjalic, T. Tsuji (Eds.), CHT01 Turbulence Heat and Mass Transfer, Aichi Shuppan Press, 2000, pp. 33–58.
[28] S. Poncet, Instabilities, Turbulence and Heat Transfer in Confined Rotating Flows, Habilitation thesis, Aix-Marseille University, 2014.
[29] S.C. Tzeng, Heat transfer in a small gap between co-axial rotating cylinders, Int. Comm. Heat Mass Transfer 33 (6) (2006) 737–743.
[30] S. Hirai, K. Takagi, K. Tanaka, T. Higashiya, Turbulent heat transfer to the flow in a concentric annulus with a rotating inner cylinder, in: Proc. of the 8th Int. Heat Transfer Conf., San Francisco, 1986.
[31] M. Bouafia, Y. Bertin, J.B. Saulnier, P. Ropert, Analyse expérimentale des transferts de chaleur en espace annulaire étroit et rainuré avec cylindre intérieur tournant, Int. J. Heat Mass Transfer 41 (10) (1998) 1279–1291.
[32] I. Kosterin, Y.P. Finat'ev, Investigation of heat transfer of a turbulent flow of air in an annular gap between rotating coaxial cylinders, INZH 8 (1963).
[33] M. Grosgeorge, Contribution à l'étude du refroidissement d'une paroi tournante par air chargé d'huile pulvérisée (Ph.D. thesis), Université de Nancy, 1983.